Optical Metasurface Generated Vector Beam for Anticounterfeiting

Chunmei Zhang, Dandan Wen, Fuyong Yue, Yuttana Intaravanne, Wei Wang,* and Xianzhong Chen†
SUPA, Institute of Photonics and Quantum Sciences, School of Engineering and Physical Sciences, Heriot-Watt University, Edinburgh EH14 4AS, UK

(Received 2 May 2018; revised manuscript received 10 July 2018; published 14 September 2018)

With the rapid development of optical metasurfaces, anticounterfeiting methods continue to evolve. Recently, the unprecedented capability of optical metasurfaces in the local manipulation of the light's polarization has been used to generate arbitrary polarization profiles, providing an unusual method for anticounterfeiting. We experimentally demonstrate a metasurface device that can hide a quick response (QR) code in the polarization profile of a laser beam. The desired space-variant polarization profile originates from the superposition of two circularly polarized light beams with opposite handedness based on a single metasurface. A linear polarizer is used to reveal the hidden QR code. The anticounterfeiting property of such a device has potential applications in product identification, item tracking, and document management.

DOI: 10.1103/PhysRevApplied.10.034028

I. INTRODUCTION

Hide-and-seek is a popular children's game in which some players conceal themselves in the environment, to be found by seekers. A spacious place is usually required in order to find more hiding places for the hiders and add more difficulty for the seekers. How to play such a game in a laser beam is very challenging due to the small cross section of the laser beam. Polarization is one of the fundamental properties of a light beam whose spatial distributions can be used to record, process, and store information. However, its practical applications have been hindered by the technical challenges in the nanoscale manipulation of the polarization profile even with the highest quality commercial devices. Metasurfaces are two-dimensional counterparts of metamaterials and have drawn much attention due to their unprecedented capability in the manipulation of amplitude, phase, and polarization at subwavelength scales [1–16]. Optical metasurfaces have been used to generate vector beams with typical polarization profiles (e.g., radial and azimuthal vector beams) [17] and arbitrary polarization profiles for hiding images [18,19], providing an unusual approach for anticounterfeiting. Quick response (QR) codes are two-dimensional barcodes usually consisting of black and white patterns with a spatially varying intensity profile, which can be processed by a QR reading machine such as a smart phone. QR codes have been widely used in many fields, including product identification, item tracking, and document management. To keep pace with continued miniaturization of devices and the daunting increase in the volume of information, new approaches to generate QR codes are desirable. Upon the illumination of a linearly polarized light beam, we experimentally demonstrate a metasurface device that can generate a light beam with an inhomogeneous polarization profile for hiding such a QR code. Unlike recently demonstrated QR code that was encoded in the spatial amplitude modulation of a light beam generated by a metasurface [20], the QR code here is hidden in the light's polarization profile. For instance, holograms are recorded interference patterns of intensity peaks and elimination of the superimposed light wave fronts, while the QR code in our work is encoded in the inhomogeneous polarization profile of a light beam with uniform intensity distribution. The reflective optical metasurface is used to generate the desired polarization distribution of the light beam. Its unique property may lead to a wide range of applications such as anticounterfeiting, encryption, and display.

II. RESULTS AND DISCUSSION

Figure 1(a) shows the schematic of our proposed approach for hiding a QR code. The vector beam that can be used to hide the QR code is generated by a reflective metasurface illuminated by a linearly polarized light beam at normal incidence. Although the resultant vector beam has a uniform intensity profile [Fig. 1(b)], which cannot be detected by our naked eyes or cameras, it has an inhomogeneous spatial polarization profile [Fig. 1(c)]. The hidden QR code [see Fig. 1(d)] is revealed by using a linear polarizer (analyzer).

Suppose the angle between the transmission axes of the analyzer and the polarizer is θ. When the completely

*w.wang@hw.ac.uk
†x.chen@hw.ac.uk

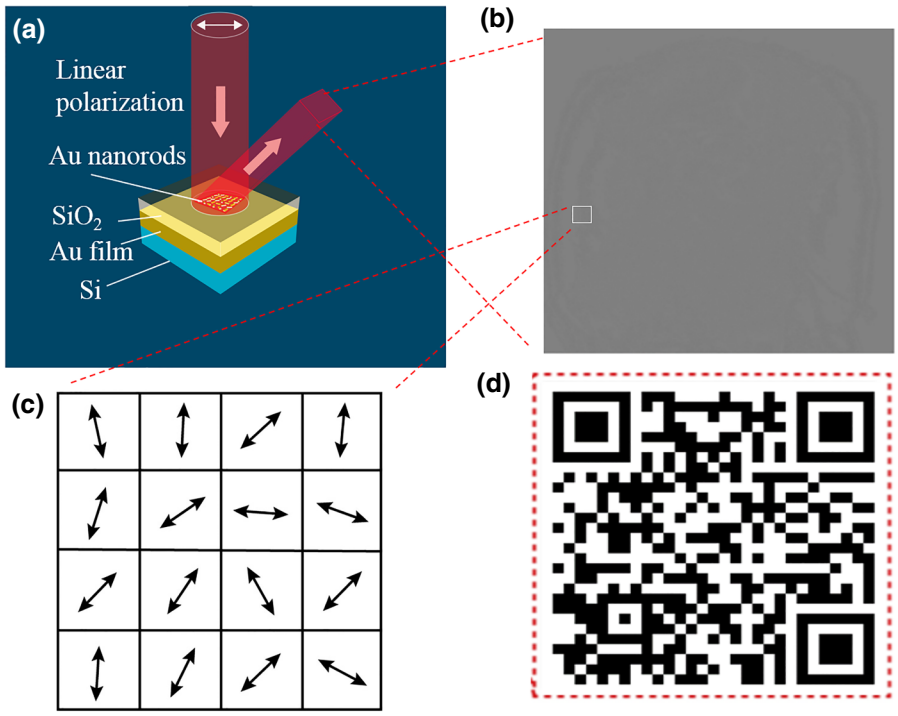

FIG. 1. Schematic of the mechanism to hide a QR code in a laser beam. (a) Schematic of the design. (b) Intensity profile. (c) Schematic of polarization distribution in the white square area in (b). (d) Target QR code.

plane-polarized light from the polarizer is incident on the analyzer, the electric field with an amplitude E_0 can be decomposed into two rectangular components, i.e., $E_0\cos\theta$ and $E_0\sin\theta$. However, the analyzer will transmit only the component ($E_0\cos\theta$) parallel to its transmission axis. Therefore, the intensity $\mathbf{I}$ of light transmitted by the analyzer is $\mathbf{I} = {E_0}^2\cos^2\theta$ (See Supplementary Section 1 in Ref. [21]). The desired polarization profile can be generated by a coherent superposition of two planar circularly polarized beams with opposite handedness that propagate along the same direction [8]. In order to ensure the coaxial propagation and make them interfere, a reflective metasurface is used to generate the desired structured beams emerging from the same metasurface, which can avoid technical hassle in the alignment system. A structured beam with an inhomogeneous polarization profile can be described as [19]

$$\boldsymbol{E}(x,y) = A\exp[i\theta(x,y)]\boldsymbol{e}_R + B\exp[-i\theta(x,y)]\boldsymbol{e}_L, \quad (1)$$

where $\boldsymbol{e}_L$ and $\boldsymbol{e}_R$ are the unit vectors of lefthand circular polarization (LCP) and righthand circular polarization (RCP). A and B denote the amplitude coefficients of RCP and LCP light and $\theta(x,y)$ represents the relative phase difference between the two orthogonal polarization states. Since the sign of the geometric phase generated at the interface of the metasurface depends on the helicity of the incident light, the two beams with opposite helicity will meet and interfere with each other, generating the desired polarization profile for the hidden QR code. Different from a common polarized laser beam, which typically has only one polarization state, different parts of the beam here have spatially variant polarization states.

The generation of desired polarization profiles with two opposite handedness and their superposition process occur on the same metasurface by controlling the polarization state of the incident light. Detailed information is available in Supplementary Section 2 [21]. To maintain high efficiency and broadband, we leverage the recent advances in the realization of high efficiency, broadband reflective-type configuration, and Pancharatnam-Berry phase metasurface to develop the designed metasurface device. Compared to other types of metasurfaces, a metasurface consisting of nanorods with spatially varying orientation shows superior phase control for the circular polarization and can ease the fabrication. The three-layer structure functions like a Fabry-Perot–like cavity, where the thickness of the SiO_2 spacer corresponds to the cavity length. Nanorods along with the spacer and the background layer function as a reflective-type half-wave plate. Detailed theoretical analysis of the broadband characteristic of such metasurfaces is available in the references [22,23]. The reflective metasurface consists of three layers: gold nanorods on the top (30 nm), a gold layer at the bottom (150 nm), and a silicon dioxide (SiO_2) spacer layer (85 nm) sandwiched between them. All the nanorods have the same geometry with various orientation angles. Each nanorod corresponds to a pixel, which has dimensions of 300 × 300 nm^2, indicating the subwavelength resolution. Each nanorod is 200 nm long, 50 nm wide, and 30 nm high. To generate the off-axis reflection (See Supplementary Section 3 in Ref. [21]), the additional phase difference between neighboring pixels

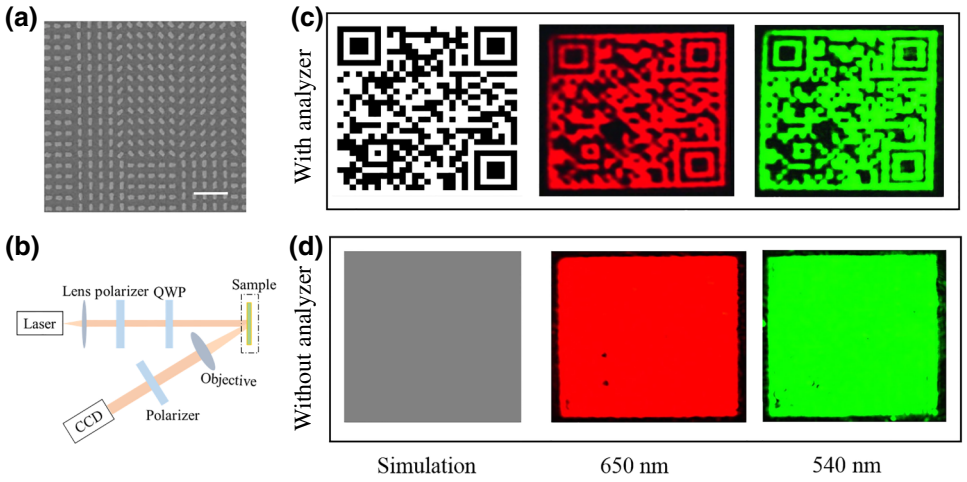

FIG. 2. Simulation and experimental results. (a) SEM image of the fabricated sample. The scale bar is 1 μm. The size of the fabricated sample is 300 $\times$ 300 μm^2. Each unit cell is 300 $\times$ 300 nm^2. (b) Schematic of experimental setup. QWP: quarter-wave plate. Simulation and experimental results (c) with and (d) without the analyzer.

of the sample along the x direction is $\pi/5$, resulting in a reflection angle of 12.2° at the incident wavelength of 650 nm. The standard electron beam lithography is used to fabricate the designed metasurface, followed by the lift-off process. For the adhesion purpose, a thin titanium layer (3 nm) is deposited on the SiO_2 layer prior to the layer for the gold nanorods. Fabrication details are available in Supplementary Section 4 [21]. The metasurface device has dimensions of 300 $\times$ 300 μm^2. Figure 2(a) shows the SEM image of the metasurface. In order to visualize the hidden QR code, an analyzer is used to reveal the hidden information in the polarization topology of the laser beam. In doing so, we do not directly observe the spatially-variant polarization profile of the laser beam, but rather indirectly confirm its existence through the intensity profile behind the analyzer and the interference fringes resulting from the right and left circular components. The experimental setup used to characterize the fabricated sample is shown in Fig. 2(b).

Figure 2(b) is the schematic of the experimental setup. To characterize the performance of the metasurfaces, a tunable laser source (NKT-SuperK EXTREME) is used to generate the desired laser beam with various polarization states after passing through a quarter-wave plate (QWP) and a polarizer in front of the sample (see Supplementary Section 5 in Ref. [21]). An objective with a magnification of 10$\times$ is used to expand the image for visualization with a CCD camera. Figures 2(c) and 2(d) show the simulation and experimental results with and without the analyzer under the illumination of linearly polarized light beams. The figures in Figs. 2(c) and 2(d) on the left, middle, and right columns represent the simulation results and experimental results at 650 and 540 nm, respectively. The slight difference between experiment and simulation is due to the imperfection of the sample and measurement error. Although the device is designed at the operating wavelength of 650 nm, it can operate in a broad wavelength range due to the broadband nature of the geometric metasurface. The experimental results at 540 nm [see right column of Figs. 2(c) and 2(d)] are given as well. The QR code contains the information of our group website (http://nanophotonicslab.eps.hw.ac.uk/), which can be

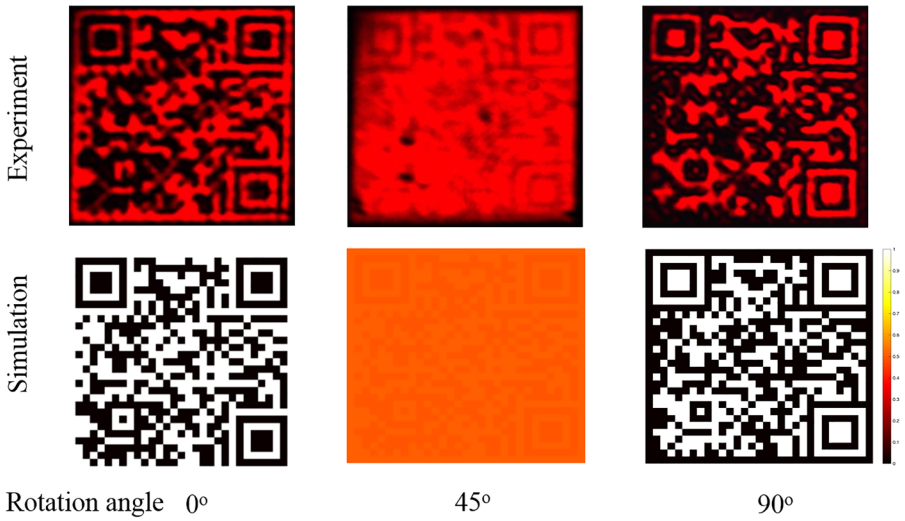

FIG. 3. The dependence of experimental results on the rotation angles of the transmission axis of the analyzer away from the vertical direction. The incident light is linearly polarized along the horizontal direction.

accessed by using a QR code reader such as a smart phone. Due to the off-axis design, another identical image is also observed in the reflected beam on the other side with respect to the surface normal.

We further characterize the device by studying the relationship between the obtained QR code images and the transmission axis of the analyzer. It is worth mentioning that the transmission axes of the polarizer (before the sample) and the analyzer (after sample) are designed along the horizontal and vertical directions, respectively. Various QR codes are obtained by rotating the transmission axis of the analyzer (designed along the vertical direction), while that of the polarizer is fixed along the horizontal direction. Figure 3 shows the simulation and experimental results when the rotation angles of the analyzer (away from the designed direction) are 0, $\pi/4$, and $\pi/2$, respectively. Interestingly, the two QR codes for the analyzer with orthogonal directions of the transmission axis (0 and $\pi/2$) are complementary images, i.e., the brightest area becomes the darkest area and vice versa. The complementary images upon changing the transmission axis of the analyzer can be explained by using Malus' law. Suppose the angle distribution between the transmission axes of the analyzer and the polarization profile of the light beam reflected by the metasurface device is $\beta(x,y)$, then the intensity of the light passing through the analyzer with a transmission axis along the horizontal direction is $I_0\cos^2\beta(x,y)$, where I_0 is the intensity of the incident light. After rotating the analyzer by 90°, the transmitted light intensity distribution will be $I_0\cos^2[\beta(x,y)+\pi/2] = I_0[1-\cos^2\beta(x,y)]$. The hidden target QR code can hardly be observed when the rotation angle is $\pi/4$.

Next, the dependence of the experimental results on the incident polarization state is investigated. Although our design is based on the incident light with linear polarization, the experimental results for other polarization states are also obtained. Various polarization states are generated by controlling the angle between the transmission axis (fixed along the x direction) of a linear polarizer and the fast axis of a quarter-wave plate. Figure 4 shows the simulation and experimental results for the incident light with linear polarization and elliptical polarization. Simulation results for other polarization states are provided in Supplementary Section 5 [21]. Obviously, the image contrast is deteriorated when the incident polarization state is away from the desired one (linear polarization). Furthermore, the generated QR code in Fig. 4(b) no longer works due to the low image contrast.

Although the metasurface approach has been used to generate an arbitrary polarization profile [18,19], the generated QR codes with unique properties are very attractive and potentially useful for both anticounterfeiting and encryption. Despite the broadband nature of the reflective metasurface, the developed device cannot operate under the illumination of white light sources since there is a slight change of the off-axis reflection at different wavelengths. The device here is demonstrated based on a reflective metasurface, but the dielectric metasurface [24] can make it work in the transmission mode, which is more compatible with most optical systems. QR codes embedded in the polarization profile of a light beam are very difficult to counterfeit due to the specialized and technologically advanced process (precise polarization control) and equipment (e.g., electron beam lithography). The simple decoding process (with a linear polarizer) can meet the verification requirements of fast speed and simplicity, which can speed up the processing of QR codes by a QR code reading machine.

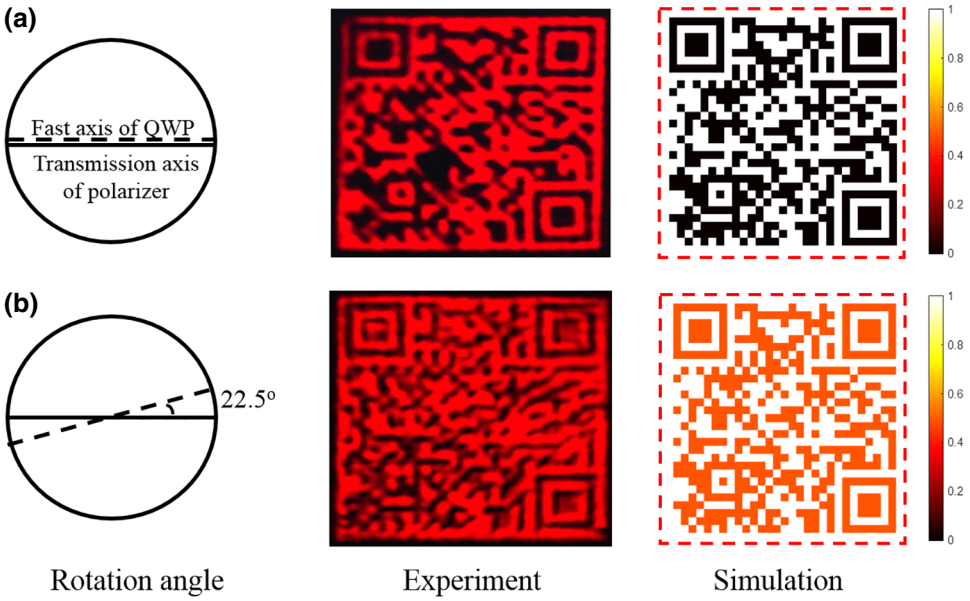

FIG. 4. The dependence of experimental results on polarization states of the incident light. The angles between the transmission axis (fixed along the horizontal direction) of a linear polarizer and the fast axis of the quarter waveplate (QWP) are 0 and $\pi/8$, respectively.

In summary, we experimentally demonstrate a metasurface device that can encode a QR code in the polarization profile of a laser beam. These hidden QR codes demonstrate the rich structure of a generated light beam by an optical metasurface that can possess subwavelength scales. The unique measurement technique used here holds great promise for anticounterfeiting and encryption, which have potential applications in product identification, item tracking, and document management.

ACKNOWLEDGMENTS

X.C. acknowledges the Engineering and Physical Sciences Research Council of the United Kingdom (Grant No. EP/P029892/1).

[1] N. Yu, P. Genevet, M. A. Kats, F. Aieta, J. P. Tetienne, F. Capasso, and Z. Gaburro, Light propagation with phase discontinuities: Generalized laws of reflection and refraction, Science **334**, 333 (2011).

[2] X. Ni, N. K. Emani, A. V. Kildishev, A. Boltasseva, and V. M. Shalaev, Broadband light bending with plasmonic nanoantenas, Science **335**, 427 (2012).

[3] L. Huang, X. Chen, H. Mühlenbernd, G. Li, B. Bai, Q. Tan, G. Jin, T. Zentgraf, and S. Zhang, Dispersionless phase discontinuities for controlling light propagation, Nano Lett. **12**, 5750 (2012).

[4] S. Sun, Q. He, S. Xiao, Q. Xu, X. Lin, and L. Zhou, Gradient-index meta-surfaces as a bridge linking propagating waves and surface waves, Nat. Mater. **11**, 426 (2012).

[5] X. Yin, Z. Ye, J. Rho, Y. Wang, and X. Zhang, Photonic spin Hall effect at metasurfaces, Science **339**, 1405 (2013).

[6] X. Chen, L. Huang, H. Mühlenbernd, G. Li, B. Bai, Q. Tan, G. Jin, C. Qiu, S. Zhang, and T. Zentgraf, Dual-polarity plasmonic metalens for visible light, Nat. Commun. **3**, 1198 (2012).

[7] G. Zheng, H. Mühlenbernd, M. Kenney, G. Li, T. Zentgraf, and S. Zhang, Metasurface holograms reaching 80% efficiency, Nat. Nanotechnol. **10**, 308 (2015).

[8] F. Yue, D. Wen, C. Zhang, B. D. Gerardot, W. Wang, S. Zhang, and X. Chen, Multichannel polarization-controllable superpositions of orbital angular momentum states, Adv. Mater. **29**, 1603838 (2017).

[9] C. Zhang, F. Yue, D. Wen, M. Chen, Z. Zhang, W. Wang, and X. Chen, Multichannel metasurface for simultaneous control of holograms and twisted light beams, ACS Photonics **4**, 1906 (2017).

[10] F. Yue, X. Zang, D. Wen, Z. Li, C. Zhang, H. Liu, B. D. Gerardot, W. Wang, G. Zheng, and X. Chen, Geometric phase generated optical illusion, Sci. Rep. **7**, 11440 (2017).

[11] D. Wen, F. Yue, C. Zhang, X. Zang, H. Liu, W. Wang, and X. Chen, Plasmonic metasurface for optical rotation, Appl. Phys. Lett. **111**, 023102 (2017).

[12] J. Burch, D. Wen, X. Chen, and A. D. Falco, Conformable holographic metasurfaces, Sci. Rep. **7**, 4520 (2017).

[13] D. Wen, F. Yue, M. Ardron, and X. Chen, Multifunctional metasurface lens for imaging and Fourier transform, Sci. Rep. **6**, 27628 (2016).

[14] X. Chen, Y. Zhang, L. Huang, and S. Zhang, Ultrathin metasurface laser beam shaper, Adv. Opt. Mater. **2**, 978 (2014).

[15] G. Li, S. Zhang, and T. Zentgraf, Nonlinear photonic metasurfaces, Nat. Rev. Mater. **2**, 17010 (2017).

[16] D. Hu, X. Wang, S. Feng, J. Ye, W. Sun, Q. Kan, P. J. Klar, and Y. Zhang, Ultrathin terahertz planar elements, Adv. Opt. Mater. **1**, 186 (2013).

[17] F. Yue, D. Wen, J. Xin, B. D. Gerardot, J. Li, and X. Chen, Vector vortex beam generation with a single plasmonic metasurface, ACS Photonics **3**, 1558 (2016).

[18] L. Wang, T. Li, R. Guo, W. Xia, X. Xu, and S. Zhu, Active display and encoding by integrated plasmonic polarizer on light-emitting-diode, Sci. Rep. **3**, 2603 (2013).

[19] F. Yue, C. Zhang, X. Zang, D. Wen, B. D. Gerardot, S. Zhang, and X. Chen, High-resolution grayscale image hidden in a laser beam, Light: Sci. Appl. **7**, e17129 (2018).

[20] A. Chanana, A. Paulsen, S. Guruswamy, and A. Nahata, Hiding multi-level multi-color images in terahertz metasurfaces, Optica **3**, 1466 (2016).

[21] See Supplemental Material at https://link.aps.org/supplemental/10.1103/PhysRevApplied.10.034028 for further details of Malus' law, polarization profile generation, off-axis reflection design, fabrication procedure of the metasurface and generation of incident light with various polarization states.

[22] S. Jiang, X. Xiong, P. Sarriugarte, S. Jiang, X. Yin, Y. Wang, R. Peng, D. Wu, R. Hillenbrand, X. Zhang, and M. Wang, Tuning the polarization state of light via time retardation with a microstructured surface, Phys. Rev. B **88**, 161104 (2013).

[23] D. Wen, F. Yue, G. Li, G. Zheng, K. Chan, S. Chen, M. Chen, K. F. Li, P. W. Wong, K. W. Cheah, E. Y. Pun, S. Zhang, and X. Chen, Helicity multiplexed broadband metasurface holograms, Nat. Commun. **6**, 8241 (2015).

[24] S. Kruk, B. Hopkins, I. I. Kravchenko, A. Miroshnichenko, D. Neshev, and Y. Kivshar, Invited Article: Broadband highly efficient dielectric metadevices for polarization control, APL Photonics **1**, 030801 (2016).